



Contents lists available at ScienceDirect

Geotextiles and Geomembranes

journal homepage: www.elsevier.com/locate/geotexmem

Linear viscoelastic behaviours of bituminous mixtures and fiberglass geogrids interfaces

Reuber Arrais Freire^{a,*}, Hervé Di Benedetto^b, Cédric Sauzéat^b, Simon Pouget^c, Didier Lesueur^d

^a University Federal of Pernambuco (UFPE), Av. Prof. Moraes Rego, 1235, Cidade Universitária, 50670-901, Recife, Pernambuco, Brazil

^b University of Lyon / ENTPE, Laboratory of Tribology and System Dynamics (LTDS) (UMR CNRS 5513), 3 Rue Maurice Audin, 69518, Vaulx-en-Velin, France

^c EFFAGE Infrastructures Research & Innovation Department, 8 rue du Dauphiné CS74005, 69964, Corbas, Cedex, France

^d Afiteixinov, 56 Route de Ferrossière, 38110 Saint-Didier-de-la-Tour, France / IMT Lille Douai, Institut Mines-Télécom, Univ. Lille, Centre for Materials and Processes, F-59000, Lille, France

ARTICLE INFO

Keywords:

Fiberglass geogrid
Reinforcement
Bituminous mixtures
Complex modulus

ABSTRACT

One major research topic is to characterize the mechanical behaviour of actual reinforced pavement structures from laboratory experimentation and take it into account for the design. This investigation aims to verify the effect of fiberglass geogrid presence on interface linear viscoelastic (LVE) behaviour separately and as a system along with the bituminous mixture layers. To conduct the research, two different fiberglass geogrids, with ultimate tensile strength (UTS) of 100 and 50 kN/m, and tack coat made of straight-run bitumen and modified by polymer were combined for the fabrication of three reinforced configurations. In addition, two unreinforced configurations were also fabricated. The first was a single layer slab and the second was a double-layered slab composed of two bituminous mixtures (same type) bonded layers by a tack coat. Complex modulus tests were carried out in specimens cored in two different directions, vertically (V) and horizontally (H) cored. The experimental data were fitted using the 2 Springs, 2 Parabolic Elements and 1 Dashpot (2S2P1D) model. The test results showed that all interfaces' complex modulus obtained for V specimens were LVE. Moreover, complex viscous properties of the interfaces were obtained from the used binder. The interface containing polymer modification presented the highest stiffness.

1. Introduction

The roadways reinforcement by geogrids has increased in the last decades in order to improve their serviceability by avoiding typical distresses occurring in these structures, such as cracking and rutting. They could be used for both rehabilitation and construction of new bituminous pavements (GMA (2002) and COST 348 (2006)). According to some authors, fiberglass geogrids are preferable for presenting high-tension resistance and flexibility at once (Nguyen et al., 2013). It is also thermally and chemically stable at mixing temperatures for bituminous mixtures (Darling and Woolstencroft 2004), and easily removable by milling in the case of further pavement maintenances. Many works have been done in the rehabilitation domain by using the geogrids reinforcement in order to control the reflective cracking and fatigue (Brown et al., 1985; De Bondt, 1999; Nguyen et al., 2013; Pasquini et al., 2015; Safavizadeh et al., 2015; Arsenie et al., 2017; Zofka et al., 2016; Noory et al., 2017; Saride and Kumar 2019). The results show generally

an improvement linked with the use of geogrids. However, in the domain of construction of new pavement, the reinforcement by geogrids is not very well explored.

Nowadays, many types of software are used for the multi-layer calculation in mechanistic-based design methods, e.g. MEPD-G (United States of America), Alizé (France), and Medina (Brazil). The geogrid reinforcement can be included as an equivalent layer if its properties (e.g. stiffness, Poison's Ratio), as well as thickness, are known. Thus, it is necessary to characterize the interface with geogrid mechanical properties in the laboratory. A great number of studies concerning destructive interface adhesion tests could be found in the literature (Tschegg et al., 2012; Ferrotti et al., 2011; Canestrari et al., 2015; Cho et al., 2016). The most used test to characterize interface adhesion is the Leutner test (Leutner 1979). This test was developed in Germany by Leutner and consisted of a direct application of shear stress. This test could be performed in specimens either fabricated in a laboratory or cored from the field (De Bondt, 1999). Another test found in

* Corresponding author.

E-mail address: reuber.freire@ufpe.br (R. Arrais Freire).

<https://doi.org/10.1016/j.geotexmem.2022.06.003>

Received 27 October 2021; Received in revised form 31 May 2022; Accepted 12 June 2022

0266-1144/© 2022 Elsevier Ltd. All rights reserved.

the literature used to characterize the adhesion of interfaces containing reinforcement by geosynthetics was the Wedge splitting test. It was conceived originally for fracture tests (Tschegg, 1986), but Tschegg et al. (2012) used it to characterize a geotextile and a geogrid reinforcement in bituminous mixtures layers. Double shear tests are also found in the literature for this same type of characterization, developed by the North Carolina State University (NCSSU) asphalt research team (Cho et al., 2016). In Italy, the Ancona Shear Testing Research and Analysis (ASTRA) was developed for the characterization of shear properties. Ferrotti et al. (2011), Canestrari et al. (2015 and 2022) used this device to characterize the shear resistance of interfaces containing reinforcement by geogrids. Attia et al. (2020 and 2021) proposed a new apparatus to characterize interfaces between bituminous mixtures called 2T3C allowing tension/compression and torsion on Hollow Cylinder. The mentioned author used the device to apply torsion and compression to hollow cylinder specimens at the same time. Digital Image Correlation technique was used to obtain the strain in the interface of double-layer specimens.

Despite the great number of studies on the shear resistance of interfaces with geogrid found in the literature, there are only a few studies concerning the rheological behaviour in the small strain domain of interfaces with geogrid where linear viscoelastic (LVE) behaviour can be considered. Cho et al. (2016) conducted a study to verify the Time-Temperature Superposition Principle to the interface shear of specimens reinforced by fiberglass geogrids. Double Shear Tester (DST) and Modified Advanced Shear Tester (MAST) were used for the shear test characterization. Digital Analysis Correlation (DIC) was used to determine interface displacement. The authors concluded that the quality of the tack coat is more important than the grid mesh opening to the shear strength. Moreover, the interfaces without geogrid presented the same shift factors as those found for bituminous mixtures complex modulus previously characterized. However, the shift factor for interfaces containing geogrids differed from the others.

Freire et al. (2018) proposed a new methodology for the determination of the linear viscoelastic (LVE) behaviour of interfaces reinforced with and without fiberglass geogrids. The authors carried out tests using two pairs of extensometers with different lengths in double-layer specimens with the same bituminous mixtures in both layers. First, a couple with 25 mm length disposed 180° from one another, and another couple with 90 mm length disposed 180° from one another. Assuming that the interface is composed of geogrid and the emulsion as an equivalent layer and using the Continuous Mechanics hypothesis, the authors obtained the complex moduli of the bituminous mixture and interface separately from the measurements. Lastly, the authors observed that the interface behaviour was LVE and it could be modelled by 2 Springs 2 Parabolic elements and 1 Dashpot (2S2P1D) model.

Solatiyan et al. (2021) conducted a work characterizing the rheological interface behaviour of interfaces containing fiberglass geogrid or not in double-layer cylindrical specimens. Traction-compression complex modulus tests were carried out using three pairs of extensometers with different lengths (25, 50, and 100 mm). The authors used a similar idea from Freire et al. (2018) to obtain the interface behaviour of specimens composed of two different bituminous mixtures layers. However, the authors analysed the complex modulus results from each pair of extensometers individually, and those were modelled using 2S2P1D. The authors concluded that considering the composite structure stiffness obtained in the laboratory as the system property could be a realistic solution to design reinforced pavements.

The investigation presented in this paper has two main goals. First, to verify the effect of fiberglass geogrid presence on interface linear viscoelastic (LVE) behaviour using the methodology proposed by Freire et al. (2018). Double-layer cylindrical specimens having the interface perpendicularly positioned in the cylinder longitudinal axis, with and without reinforcement, were used. Then, this investigation aims at evaluating the geogrid and tack coat effect on specimens having the interface parallel positioned in the cylinder longitudinal axis, subjected

to small strain amplitude loading.

2. Materials and experimental protocol

2.1. Materials

The French bituminous mixture called BBSG 0/10 (*Béton Bitumineux Semi-Grenu*) was used to conduct the experimental campaign. This mixture was classified according to the European standards (NF EN 13108-1, 2016) and is generally used for surface courses in France. The BBSG 0/10 gradation curve is presented in Fig. 1(a). It is composed of rhyodacite and rhyolitic mineral aggregates, limestone filler, and 20% of reclaimed asphalt pavement (RAP) containing 4.75% of aged bituminous binder. These aggregates were mixed with 4.40% of a new bituminous binder classified as 35/50 by its penetration. The total bituminous binder content (aged plus new) in the mixture was 5.53% per total weight of the mixture.

The geogrids used to reinforce the bituminous mixtures were Notex Glass®, presented in Fig. 1(b). It was composed of fiberglass yarns knitted to a light polyester veil, with a bituminous coating on both sides. The grids had a square mesh opening of 25 mm in the two directions. Two types of geogrids were used in this work with ultimate tensile strength (UTS) of 50 kN/m (C 50/50) and 100 kN/m (C 100/100), in the two perpendicular directions. These UTS were obtained at the failure point of 3% of strain in grid tensile characterization tests carried out for fabrication quality control. Lastly, a bituminous emulsion 160/220 by penetration (NF EN 12591) was used as a tack coat to bond the geogrid in the middle part of the slabs. This emulsion has the industrial name Actimul®, and it was prepared with 65% of residual bitumen. Moreover, a different type of bituminous emulsion was used, called by the industrial name Emulprene®. It was prepared with 64% of residual bitumen with 160/220 penetration, and modified with 2.6% of styrene-butadiene-styrene (SBS) block copolymer.

2.2. Specimens preparation

Five different slab configurations, with dimensions 600 (length), 400 (width), and 150 mm (depth), were compacted using a French wheel compactor (NF EN 12697-33, 2019). Configuration A did not have an interface, while B, C, D, and E had an interface and were denoted by double-layer slabs. Configuration B had only the tack coat of emulsion made of straight-run bitumen at a residual rate of 290 g/m². Whereas configurations C, D, and E were made with geogrid (50 and 100 kN/m of UTS) and the tack coat (straight-run bitumen emulsion and with SBS) at a residual rate of 800 g/m², and were denoted by reinforced slabs.

The fabrication of configuration A slab followed the classical procedure described in the standard (NF EN 12697-33, 2019), since it was composed of a single layer slab, without interface/reinforcement. Concerning the reinforced slabs, they were fabricated by first compacting a half-height slab (75 mm) at a temperature of 180 °C (for mixing and compaction) and cooling down for 24h. Then, the first tack coat application was done (400 g/m²), followed by the geogrid placement. Afterwards, the second tack coat application was done (400 g/m²) on the geogrid surface. A period of 24h waited so that the breaking process occurs in the emulsion before the second half-height (75 mm) slab compaction.

From each slab, cylindrical specimens were cored with a minimum waiting time of two weeks after the fabrication. They were cored with 75 mm diameter and 140 mm height and in two different coring directions. Specimens named H were horizontally cored, in relation to the roller compaction direction, while those named V were vertically cored. Fig. 2 presents the coring plan for each slab, detailing the final cored specimens and their interface positions. Table 1 presents the details of the interface and air voids of each slab configuration and tested specimen.

Complex modulus tests were performed using a hydraulic press

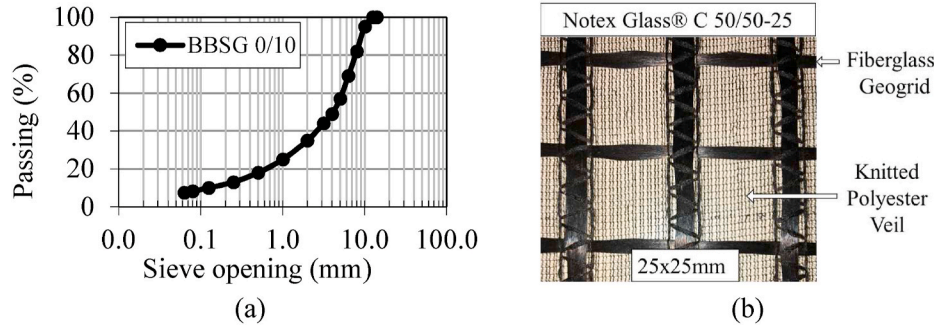


Fig. 1. Components of tested specimen: (a) Bituminous mixture gradation curve and (b) fiberglass geogrid Notex Glass® 50/50-25.

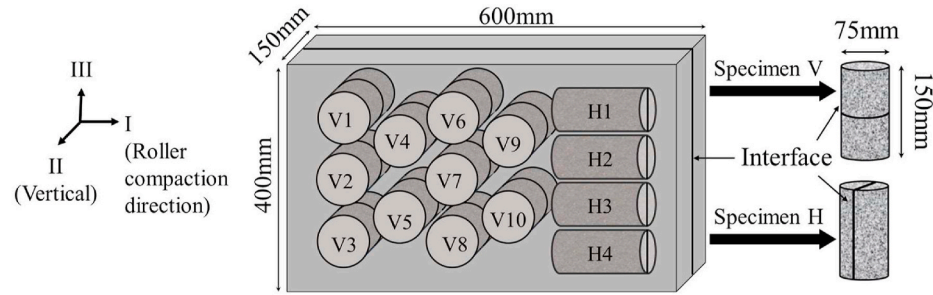


Fig. 2. Slabs coring plan and interface (with or without geogrid) position illustration for specimens V and H.

Table 1

Tested specimens' composition and air voids measured in the bituminous mixture layers.

Slab configuration	Specimen	Interface		Air Voids (in bituminous mixture layers) (%)
		Composition	Tack coat rate (residual binder)	
A	A1-H3	No interface		6.2
	A1-H4			6.0
	A1-V2			8.5
	A1-V5			8.6
	B1-H1			Straight-run bitumen
B1-H2	6.1			
B2-V1	6.8			
B	B2-V2			6.3
	C2-H1	Straight-run bitumen and GG	2 × 400 g/m ²	7.8
	C2-H3			7.3
	C1-V6	100 kN/m		8.3
	C2-V1			7.1
D	D1-H1	Straight-run bitumen and GG		8.7
	D1-H3			7.3
	D2-V1	50 kN/m		6.0
	D2-V3			6.9
	E	E1-H1	Modified bitumen and GG	
E1-H2		6.4		
E2-V4		100 kN/m		6.8
E2-V5				6.7

GG 100 kN: Geogrid Notex Glass® C 100/100–25; and GG 50 kN: Geogrid Notex Glass® C 50/50-25.

(INSTRON). This press has a maximum force capacity of ±25 kN on the actuator. A thermal chamber was used for temperature control during the tests. The tests were carried out by applying axial tension-compression sinusoidal loading with a controlled strain amplitude (ϵ_0) of 50 $\mu\text{m}/\text{m}$ (100 $\mu\text{m}/\text{m}$ peak to peak) and a mean value of zero. During the test, the stress amplitude (σ_0) was measured with the aid of the load cell. Equation (1) presents the sinusoidal axial strain loading ($\epsilon(t)$) and Equation (2) presents the sinusoidal axial stress response ($\sigma(t)$) with the

phase angle (φ) between strain and stress signals, typically observed in viscoelastic materials.

$$\epsilon(t) = \epsilon_0 \cdot \sin(\omega t) \quad (1)$$

$$\sigma(t) = \sigma_0 \cdot \sin(\omega t + \varphi) \quad (2)$$

The axial deformation measurements were done by four extensometers, a couple with 25 mm length (l_1) disposed 180° from one another, and another couple with 90 mm length (l_2) disposed 180° from one another (see Fig. 3), both fixed in the middle height of specimens. The strain amplitude commanded during the test was calculated by the average of the two smaller extensometers (25 mm). The temperature is measured by a thermal gauge (PT100 temperature probe) fixed on the specimen surface. Fig. 3 presents the instrumentation for this test.

The test was carried out at nine temperatures: -25, -15, -5, 5, 15, 25, 35, 45 and 52 °C and eight frequencies: 0.003, 0.01, 0.03, 0.1, 0.3, 1, 3 and 10Hz, following the same procedure described in Phan et al. (2017). Equation (3) presents the complex modulus (E^*) calculation, where $|E^*|$ is its norm.

$$E^* = \frac{\sigma_0}{\epsilon_0} e^{-i\varphi} = |E^*| e^{-i\varphi} \quad (3)$$

2.3. Interface LVE analysis methodology (V specimens)

The method used to characterize the interfaces of specimen V was the one proposed by Freire et al. (2018). Two approaches were used to characterize the bituminous mixture and the interface of specimen V during the complex modulus test. The first one is a bulk approach that uses the continuum mechanics hypothesis. The second one assumes that the interface is infinitely thin. The first interface analysis was done by considering the geogrid and the emulsion used to bond the geogrid in the specimen as an equivalent layer with a thickness (t) as shown in Fig. 4.

It is possible to show (Freire et al., 2018) that the complex modulus measurements obtained from each pair of extensometers (E_1^* (for extensometers l_1) and E_2^* (for extensometers l_2)) considering a homogeneous material is a combination of the bituminous mixture modulus (E_A^*)

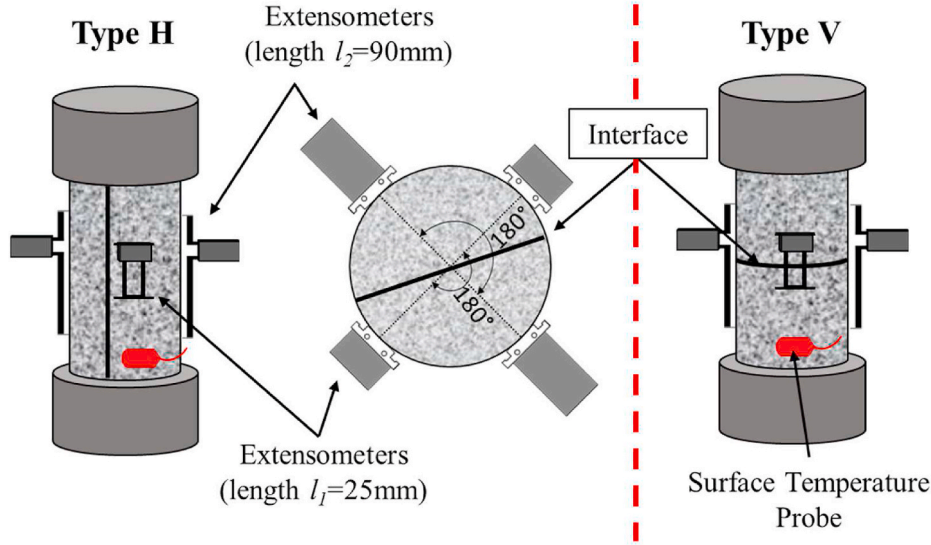


Fig. 3. Illustration of experimental instrumentation and apparatus for H and V type samples.

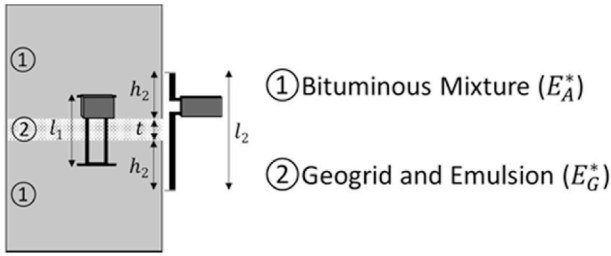


Fig. 4. Continuous Mechanics interface calculation hypothesis scheme.

and the interface modulus (E_G^*). Thus, from the measurements obtained from the extensometers l_1 and l_2 , it was possible to obtain E_A^* according to Equation (4). Then, E_G^* could be calculated for any chosen thicknesses values (t) using Equation (5).

$$E_A^* = \frac{(l_2 - l_1) \cdot E_1^* \cdot E_2^*}{l_2 \cdot E_1^* - l_1 \cdot E_2^*} \quad (4)$$

$$E_G^*(t) = \frac{t \cdot E_i^* \cdot E_A^*}{l_i \cdot E_A^* - (l_i - t) \cdot E_i^*} \quad \text{with } i = 1 \text{ or } 2 \quad (5)$$

The second interface analysis approach was performed by assuming the interface as a film with no thickness. In this case, the behaviour could be represented by an interface stiffness (K_G^*) linking σ^* and vertical displacement observed between the interfaces of the two bituminous mixtures layers. Then, K_G^* could be obtained according to Equation (6). More details regarding this method can be found in Freire et al. (2018).

$$K_G^* = \left(\frac{E_G^*}{t} \right) \left[\text{when } t \rightarrow 0 \right] = \frac{E_A^*}{l_i \cdot \left(\frac{E_i^*}{E_A^*} - 1 \right)} \quad \text{with } i = 1 \text{ or } 2 \quad (6)$$

2.4. 2S2P1D LVE model

All experimental LVE behaviour obtained for the five configurations was modelled using the 2S2P1D rheological model. This model was developed at the University of Lyon/ENTPE and it consists of 2 springs (elastic elements), 2 parabolic creep elements and 1 dashpot (purely viscous) (Di Benedetto et al., 2007; Olard and Di Benedetto, 2003). Seven coefficients were used to fit the experimental data and the value of the complex modulus given by the model was calculated by Equation

(7), for any frequency f and temperature T .

$$E^*(i\omega\tau) = E_{00} + \frac{E_0 - E_{00}}{1 + \delta(i\omega\tau)^{-k} + (i\omega\tau)^{-h} + (i\omega\beta\tau)^{-1}} \quad (7)$$

Where the pulsation $\omega = 2\pi f$ with f the loading frequency. E_{00} is the static modulus, obtained in higher temperatures (or lower frequencies). E_0 is the glassy modulus, obtained at the lower temperatures (or higher frequencies). Moreover, k , h and δ are calibration constants. Finally, τ is the characteristic time and depends on the temperature T , and β is a constant that depends on the dashpot viscosity ($\eta = (E_0 - E_{00})\beta\tau$). To remove the effects of E_0 and E_{00} , a normalization (Pouget et al., 2010; Pham et al., 2015) can be performed according to Equation (8). This expression of the normalized complex modulus E_{norm}^* characterizes the complex viscous properties.

$$E_{norm}^* = \frac{E^* - E_{00}}{E_0 - E_{00}} = \frac{1}{1 + \delta(i\omega\tau)^{-k} + (i\omega\tau)^{-h} + (i\omega\beta\tau)^{-1}} \quad (8)$$

3. Experimental results & analysis

This section is separated into three parts. The first sub-section presents the results for bituminous mixtures only. Then, only E_A^* is presented for type V double-layer specimen. A classical complex modulus analysis is done for single layer specimens (configuration A) and double-layer specimens type H. The second sub-section focus on the interface LVE behaviour of the double-layer specimens type V. The last sub-section presents the results obtained concerning the reinforced specimens type H and the geogrid contribution evaluation during the tests.

3.1. Bituminous mixture complex modulus results and modelling

Fig. 5(a) presents the bituminous mixtures' complex modulus test results in the Cole-Cole plan concerning the specimens type V. Therefore, only the E_A^* was plotted for the specimens with an interface. Fig. 5 (b) presents the complex modulus test results in the Cole-Cole plan concerning the specimens type H. In this case, a classical analysis was done with test results (axial strain obtained from the average of four extensometers). Moreover, for both graphics (V and H), the 2S2P1D model for each specimen was also plotted and the coefficients used in the calibration are presented in Table 2. From Cole-Cole plan curves (see Fig. 5), it could be noticed that a unique curve was obtained when changing frequency and temperature for each specimen test result for both coring directions (V and H). Therefore, the results indicated that

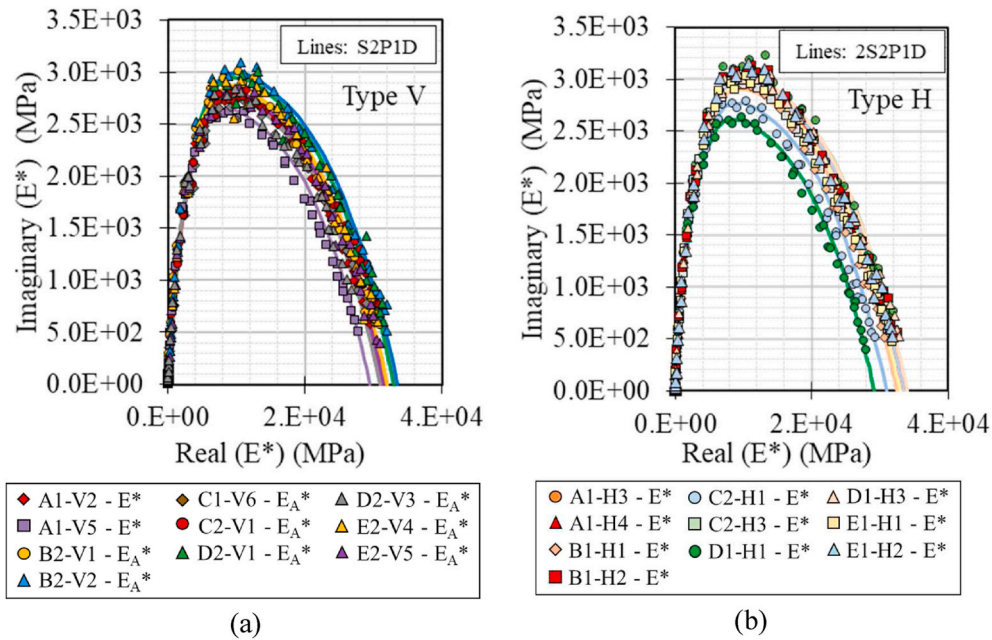


Fig. 5. Bituminous mixtures complex modulus test results in Cole-Cole plan with 2S2P1D model for each test for: (a) type V samples (E_A^*) and (b) type H samples.

Table 2

Bituminous Mixture 2S2P1D constants obtained from the different tested specimens (with and without geogrid cored in H or V direction).

Specimen	E_{00} (MPa)	E_0 (MPa)	τ (s) (T_{ref} 15 °C)	k	h	δ	β
A1-V2	15.0	3.12E+04	0.27	0.185	0.60	2.35	200
A1-V5	10.5	2.95E+04					
A1-H3	25.0	3.40E+04					
A1-H4	10.0	3.33E+04					
B2-V1	12.0	3.20E+04	0.40				
E_A^*							
B2-V2	30.0	3.35E+04	0.27				
E_A^*							
B1-H1	6.0	3.25E+04	0.32				
B1-H2	15.0	3.35E+04	0.40				
C1-V6	50.0	3.10E+04	0.50				
E_A^*							
C2-V1	60.0	3.20E+04					
E_A^*							
C2-H1	13.0	3.10E+04	0.30				
C2-H3	20.0	3.25E+04	0.50				
D2-V1	35.0	3.30E+04	0.40				
E_A^*							
D2-V3	15.0	3.10E+04					
E_A^*							
D1-H1	7.0	2.92E+04					
D1-H3	10.0	3.40E+04					
E2-V4	20.0	3.20E+04	0.50				
E_A^*							
E2-V5	25.0	3.15E+04					
E_A^*							
E1-H1	10.0	3.30E+04	0.40				
E1-H2	10.0	3.35E+04					

the material could be considered thermoreologically simple, and the time-temperature superposition principle (tTSP) was validated for all tested specimens.

Although all specimens contained the same bituminous mixture, the results presented in Fig. 5 were not superposed. However, the same shape coefficients of the 2S2P1D model (k , h , δ , and β) were obtained for all specimens, as observed in Table 2. The difference in the results was related to the glassy modulus (E_0) and static modulus (E_{00}) only, which could be explained by the voids content of the specimens (Fig. 6). E_0

values were plotted against the air voids content of the specimen in Fig. 6. The red squares stand for the specimens type H, and the red pointed line is the linear fit done for those specimens. The blue circles stand for the specimens type V, and the blue dash line is the linear fit for V. Finally, the black line is the linear fit for all the tested specimens.

The linear fit obtained for specimens V was worse than the fit obtained for specimens H, since the R^2 was 67.6% for specimens V, while the R^2 for specimens H was 86.8%. Thus, it could be observed that the variation of E_0 was highly related to the air voids variation on the specimens. This statement agrees with the previous works conducted by the LTDS/ENTPE team (Pham et al., 2015; Cardona et al., 2016; Pedraza et al., 2019). In addition, the difference observed between the linear fit obtained for specimens type H and V was due to the material anisotropy. However, this difference was approximately 5%, and, thus, can be considered negligible.

Nonetheless, the glassy modulus (E_0) and static modulus (E_{00}) are parameters that vary from sample to sample in the function of their particularities. To compare the LVE behaviour of the tested specimens, the normalization described in Equation (8) was performed. Fig. 7 presents the normalized complex modulus test results of all specimens (V and H) with the 2S2P1D model in the Cole-Cole plan.

From the normalized curves, it can be observed that there was a superposition in all experimental data. This superposition observed indicates that all specimens presented similar LVE behaviour, the same results observed in Freire et al. (2018). This result was expected since the same bituminous mixture constituted all specimens. Moreover, this result corroborates the effectiveness of the analysis proposed method. Finally, good repeatability was verified for the tested specimens.

3.2. Interfaces complex modulus results and modelling of V specimens

In order to analyse the interfaces behaviour of specimens V, the interface stiffness (K_G^*) (equation (6)) was used since it is not dependent on an arbitrarily chosen thickness (which is not the case for interface moduli E_G^* , Equation (5)). Fig. 8(a) presents all interface stiffness test results in the Cole-Cole plan with the 2S2P1D model simulations. Fig. 8 (b) presents the glassy modulus (K_{G0}) obtained for each interface studied.

From Fig. 8, it can be observed that the specimens in configuration B (interface with straight-run bitumen emulsion only) presented higher

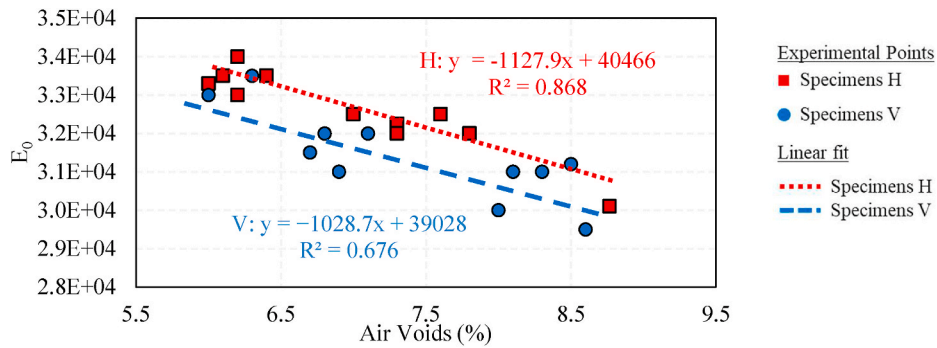


Fig. 6. Bituminous mixture glassy modulus (E_0) versus voids content for all tested specimens.

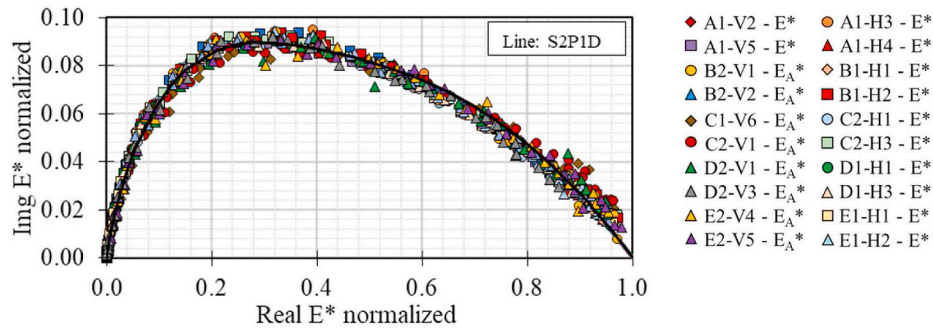


Fig. 7. Bituminous mixtures complex modulus test results of all specimens in normalized Cole-Cole plan.

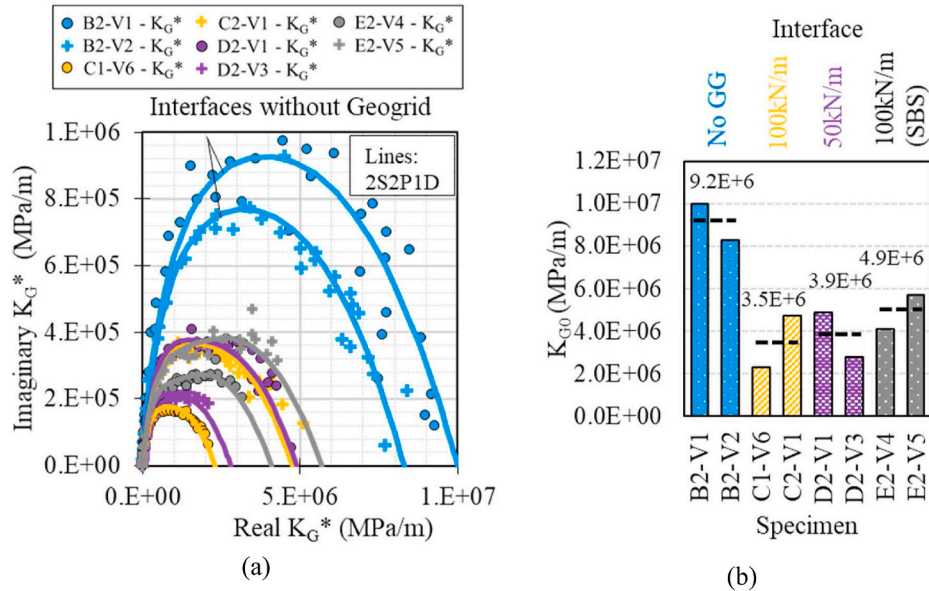


Fig. 8. Interface stiffness (K_G^*) test results: (a) Cole-Cole plan; (b) K_{G0} obtained for each tested specimen.

stiffness when compared to the other configurations having geogrid. This result can be explained by the higher quantity of tack coat used for specimens with geogrid (twice 400 g/m^2 versus 292 g/m^2 of residual binder), which gives a thicker binder interface. Concerning the reinforcement specimens, configurations C (geogrid of 100 kN/m and straight-run bitumen emulsion) and D (geogrid of 50 kN/m and straight-run bitumen emulsion) presented similar interface stiffness. However, configuration E (geogrid of 100 kN with modified emulsion bitumen) presented the highest stiffness interface among the reinforced ones. Thus, the quality of the emulsion created stiffer interfaces between

bituminous mixtures reinforced by fiberglass geogrid. This result corroborates with the work done by Cho et al. (2016), showing that the tack coat quality can overlap the influence of geogrid type.

Table 3 presents all the 2S2P1D model coefficients calibrated for K_G^* . The behaviour of all interfaces was LVE and could be modelled using the 2S2P1D model. It can be noticed that not only the glassy modulus (K_{G0}) and static modulus (K_{G00}) were different but also the shape coefficients of the 2S2P1D model (k , h , δ , and β) were different for the interfaces studied. Comparing configurations C and D, identical shape coefficients could be considered. Moreover, SBS modification in

Table 3
Interface stiffness (K_G^*) 2S2P1D constants obtained from the different tested specimens (with and without geogrid cored in V direction).

Specimen	K_{G00} (MPa/m)	K_{G0} (MPa/m)	k	h	δ	τ (s) (15 °C)	β
B2-V1	4000	1.00E+07	0.210	0.590	2.80	0.200	30
B2-V2	7000	8.30E+06				0.100	
C1-V6	800	2.30E+06	0.175		3.00	0.030	200
C2-V1	1300	4.75E+06					
D2-V1	888	4.90E+06					
D2-V3	500	2.80E+06					
E2-V4	400	4.10E+06	0.165		3.70	0.007	500
E2-V5	700	5.70E+06				0.011	

configuration E and the lack of geogrid in configuration B yield considerable variation in interface LVE behaviour. This result indicates that the bitumen type and amount play an important role in interface LVE behaviour.

Once again, the glassy modulus (K_{G0}) and static modulus (K_{G00}) influences were removed by performing the normalization described in Equation (8). Fig. 9 presents interfaces K_G^* in the normalized Cole-Cole plan. Interfaces of configurations C and D, having the same tack coat type and rate (straight-run bitumen emulsion and 800 g/m², respectively) presented overlapped curves. Interfaces of configuration E (modified bitumen) and configuration B (composed of straight-run bitumen emulsion at a rate of 290 g/m² and without geogrid), having different tack coat types and rates presented distinct curves (Fig. 9). This result suggests that the interface LVE behaviour was majorly affected by the bitumen type and rate, rather than the fiberglass geogrid UTS and presence.

3.3. Influence of fiberglass geogrid on H specimen's behaviour

Specimens type H have the geogrid/interface oriented in the axial loading direction. Assuming that the complex modulus measured (E_M^*) during the test is a composition of the bituminous mixtures complex modulus (E_A^*) plus the geogrid stiffness ($k_{G,SPC}$). However, the geogrid stiffness does not have a viscous component, since it is an elastic material. Thus, the complex modulus of bituminous mixtures can be obtained using Equation (9), which indicates that the measured load is the sum of the load taken by the bituminous mixture and the one taken by the geogrid. Moreover, assuming that the geogrid could be not entirely mobilized during the test, a constant C was included in Equation (9) representing the percentage of possible geogrid mobilization.

$$E_A^* = E_{M1} - C \frac{k_{G,SPC}}{S} + iE_{M2} \tag{9}$$

Where S stands for the area of the specimen section, E_{M1} is the elastic

part, E_{M2} is the viscous part of the measurement and i the imaginary unit of a complex number. To calculate $k_{G,SPC}$ for each type of fiberglass geogrid, their UTS characterization tests were considered. For example, concerning Notex Glass® C 100/100-25, its UTS of 100 kN/m was divided by 3%, which was the strain measured corresponding to 100 kN/m. Then, it was multiplied by the number of yarns within the specimen (3) and divided by the number of yarns per linear meter (40). Therefore, the $k_{G,SPC}$ yielded for the mentioned grid was approximately 61 MPa. Consequently, the one for Notex Glass® C 50/50-25 should be half of this value, 30.5 MPa, since both have the same geometry and achieve their UTS at 3% of strain.

In order to obtain the actual percentage of geogrid mobilization during the complex modulus tests, two hypotheses were tested: (i) the geogrid was fully mobilized ($C = 100\%$) and (ii) the geogrid was not mobilized ($C = 0\%$). Then, the results were plotted with the results obtained for the specimens without geogrid (A1-H3, A1-H4, B1-H1, and B1-H2) in Black space in Fig. 10. It was observed that the unreinforced specimens presented similar curve shapes, having a peak of phase angle value between 35 and 45 °C, classically obtained for bituminous mixtures. The geogrid influence was only noticeable at high temperatures since at low temperatures the bituminous mixture has a high modulus that overlaps the geogrid contribution. However, considering the hypothesis of full geogrid mobilization ($C = 100\%$), the curve presented a dissimilar behaviour of phase angle obtained in bituminous mixtures characterization. Thus, to define a criterion of geogrid mobilization, a threshold of 62° of phase angle was considered an acceptable limit for bituminous mixtures behaviour. Then, simulations of different percentages of C were done to find out its maximum possible value (C_{MAX}) that respects the chosen criterion. This value represents the real percentage of geogrid mobilization of the analysed specimen. Regarding C2-H1, C_{MAX} was equal to 18%, as can be also seen in Fig. 10.

The same simulation was done for all reinforced specimens and C_{MAX} was obtained. Fig. 11 presents the percentage of geogrid mobilization in the complex modulus test concerning specimens H for each studied specimen configuration.

From the previous figure, configuration C (geogrid of 100 kN/m and straight-run bitumen emulsion) presented the highest geogrid mobilization level and configuration E presented the lowest geogrid mobilization level. However, the specimens presented considerably low geogrid mobilization levels when subjected to small strain amplitudes tension-compression tests, especially configuration E (8 and 10%). Two explanations could be used to explain this result. First, a geogrid slippage could have occurred within the interface during testing. At high temperatures, the bitumen tack coat presents low stiffness that could facilitate the geogrid slippage during loading cycles. Second, the geogrid was not tensioned within the sample at the beginning of the test. In this case, just after a certain amount of strain loading, it began to be properly tensioned and, then, provided any contribution to loading support.

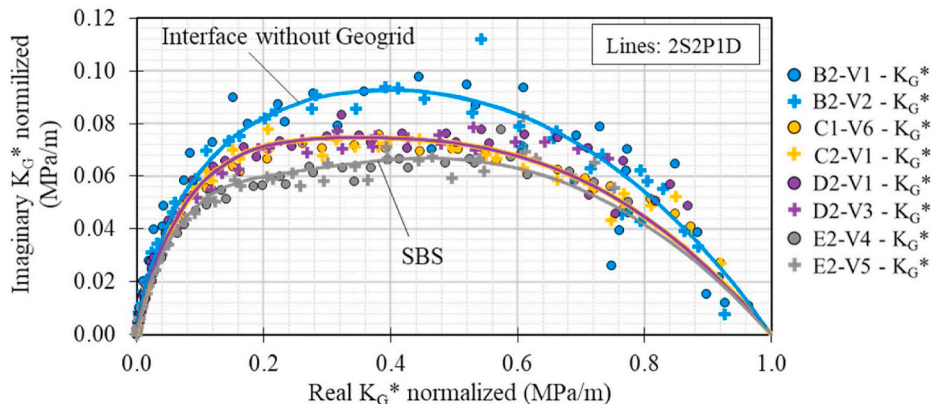


Fig. 9. Interface stiffness (K_G^*) test results of all interfaces in normalized Cole-Cole plan.

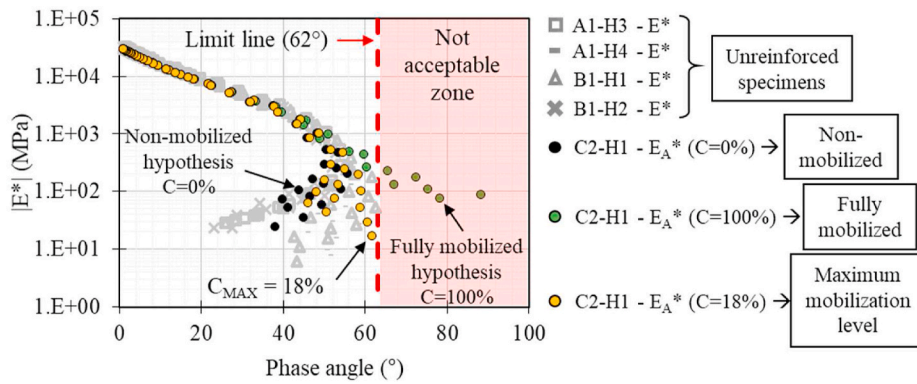


Fig. 10. Results in black space of specimen C2–H1 considering different percentages of geogrid mobilization (C = 0, 18, and 100%) plotted with the unreinforced specimens.

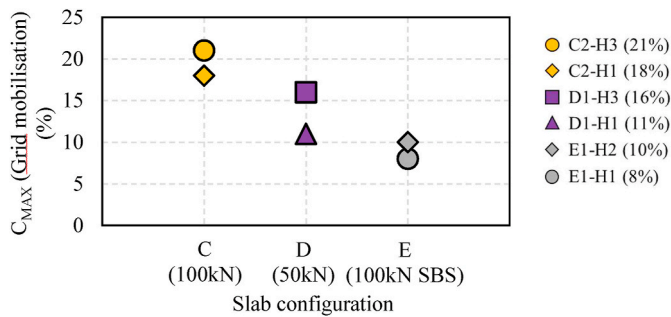


Fig. 11. Maximum geogrid mobilization in specimens H during complex modulus test for each slab configuration.

Therefore, the trend observed in test results would be not related to the geogrid UTS or tack coat presented in the specimens, but interfaces specificities due to slab fabrication.

4. Conclusions and perspectives

In this work, the methodology proposed by Freire et al. (2018) was used to verify the fiberglass geogrid presence, type and tack coat on interface linear viscoelastic (LVE) behaviour. Moreover, the geogrid effect on specimens having the interface parallel positioned in the cylinder longitudinal axis, subjected to small strain amplitude loading, was evaluated. The major conclusions are listed below:

- The method proposed by Freire et al. (2018) was confirmed in this study to be a reliable tool for interface LVE characterization including interface with geogrid reinforcement.
- The bituminous mixture layers' complex modulus (E_A^*) of reinforced specimens type V was successfully obtained and their LVE behaviour was the same as those obtained for mixtures without reinforcement.
- The interface stiffness (K_G^*) obtained in type V specimens analysis was LVE and it could be modelled by 2S2PD.
- Specimens type V from configuration B (interface with straight-run bitumen emulsion only) presented the highest interface stiffness (K_G^*). However, the specimens from this configuration had a much thinner interface due to the quantity of tack coat in the interface, 292 g/m² versus 800/m² of residual binder in reinforced specimens.
- Interface normalized curves suggest that the interface LVE behaviour was majorly affected by the tack coat type and rate, rather than the fiberglass geogrid UTS. Bitumen type and amount play an important role in interface LVE behaviour.
- The tack coat containing SBS-modified bitumen increased the interface stiffness (K_G^*) of reinforced type V specimens

- Considerable low level of geogrid mobilization was obtained at small strain amplitudes tension-compression tests concerning specimens horizontally cored. Especially for specimens with interface with modified bitumen.

Declaration of competing interest

The authors declare that they have no known competing financial interests or personal relationships that could have appeared to influence the work reported in this paper.

Acknowledgments

The authors express their sincere gratitude to the Brazilian public organization CNPq (*Conselho Nacional de Desenvolvimento Científico e Tecnológico*) for providing the PhD grant of first author, and the French companies EIFFAGE Infrastructures and Afiteixinov for the technical and financial support, and material providing.

References

Arsenie, I.M., Chazallon, C., Duchez, J.L., Hornych, P., 2017. Laboratory characterisation of the fatigue behaviour of a glass fibre grid-reinforced asphalt concrete using 4PB tests. *Road Mater. Pavement Des.* 18 (1), 168–180. <https://doi.org/10.1080/14680629.2016.1163280>.

Attia, T., Di Benedetto, H., Sauzéat, C., Pouget, S., 2020. 2T3C HCA, a new hollow cylinder device using Digital Image Correlation to measure properties of interfaces between asphalt layers. *Construct. Build. Mater.* 247, 118499 <https://doi.org/10.1016/j.conbuildmat.2020.118499>.

Attia, T., Di Benedetto, H., Sauzéat, C., Pouget, S., 2021. Behaviour of an interface between pavement layers obtained using Digital Image Correlation. *Mater. Struct.* 54, 38. <https://doi.org/10.1617/s11527-021-01625-w>.

Brown, S.F., Brunton, J.M., Hughes, D.A.B., Brodrick, B.V., 1985. Polymer grid reinforcement of asphalt. *Proc. Ass. Asphalt Paving Technol.* 54, 18–41.

Canestrari, F., Belogi, L., Ferrotti, G., Graziani, A., 2015. Shear and flexural characterization of grid-reinforced asphalt pavements and relation with field distress evolution". *Mater. Struct.* 48 (4), 959–975. <https://doi.org/10.1617/s11527-013-0207-1>, 2015.

Canestrari, F., Cardone, F., Gaudenzi, E., Chiola, D., Gasbarro, N., Ferrotti, G., 2022. In: Interlayer bonding characterization of interfaces reinforced with geocomposites in field applications" *Geotextiles and Geomembranes*, 50, pp. 154–162. <https://doi.org/10.1016/j.geotextmem.2021.09.010>. ISSN 0266-1144, 1.

Cho, S.H., Safavizadeh, S.A., Kim, Y.R., 2016. Verification of the applicability of the tTsp principle to interface shear stiffness and strength of GlasGrid reinforced asphalt mixtures. *Road Mater. Pavement Des.* 18 (4), 766–784. <https://doi.org/10.1080/14680629.2016.1189350>.

Cost Action 348, 2006. Final Report of a European Concerted Research Action Designated as COST Action 348 "Reinforcement of Pavements with Steel Meshes and Geosynthetics (REIPAS).

Darling, J.R., Woolstencroft, J.H., 2004. A study of fiberglass pavement reinforcement used in different climatic zones and their effectiveness in retarding reflective cracking in asphalt overlays. In: *Proceedings of the 5th International RILEM Conference on Cracking in Pavements*, Limoges.

De Bondt, A.H., 1999. *Anti-reflective Cracking Design of Reinforced Asphaltic Overlays*", PhD Thesis. Delft University of Technology, Netherland.

- Di Benedetto, H., Neifar, M., Sauzéat, C., Olard, F., 2007. Three-dimensional thermo-viscoplastic behaviour of bituminous materials: the DBN model. *Road Mater. Pavement Des.* 8 (2), 285–316.
- Ferrotti, G., Canestrari, F., Virgili, A., Grilli, A., 2011. A strategic laboratory approach for the performance investigation of geogrids in flexible pavements. *Construct. Build. Mater.* 25 (5), 2343–2348. <https://doi.org/10.1016/j.conbuildmat.2010.11.032>.
- Freire, R.A., Di Benedetto, H., Sauzéat, C., Pouget, S., Lesueur, D., 2018. Linear viscoelastic behaviour of geogrids interface within bituminous mixtures. *KSCE J. Civ. Eng.* 22 (6), 2082–2088. <https://doi.org/10.1007/s12205-018-1696-9>.
- Geosynthetic Material Association, 2002. *Handbook of Geosynthetics*. USA.
- Leutner, R., 1979. *Untersuchung des Schichtenverbundes beim bituminösen Oberbau*. Bitumen 41–3, 84–91 (In German).
- NF EN 12591, 2009. "Bitumen and Bituminous binders." Specifications for Paving Grade Bitumens. Association Française de Normalisation (AFNOR), Paris (In French).
- NF EN 12697-33, 2019. Bituminous Mixtures - Test Method - Part 33: Specimen Prepared by Roller Compactor. Association Française de Normalisation (AFNOR), Paris (In French).
- NF EN 13108-1, 2016. Mélanges bitumineux. Spécifications pour le matériau. Association Française de Normalisation (AFNOR), Paris (In French).
- Nguyen, M.L., Blanca, J., Kerzréhoa, J.P., Hornych, P., 2013. Review of glass fibre grid use for pavement reinforcement and APT experiments at IFSTTAR. *Road Mater. Pavement* 14 (1), 287–308.
- Noory, A., Nejad, F.M., Khodaii, A., 2017. Effective parameters on interface failure in a geocomposite reinforced multilayered asphalt system. *Road Mater. Pavement Des.* <https://doi.org/10.1080/14680629.2017.1305435>.
- Olard, F., Di Benedetto, H., 2003. General '2S2P1D' model and relation between the linear viscoelastic behaviours of bituminous binders and mixes. *Road Mater. Pavement Des.* 4 (2), 185–224. Jan. 2003.
- Pasquini, E., Pasetto, M., Canestrari, F., 2015. Geocomposites against reflective cracking in asphalt pavements: laboratory simulation of a field application. *Road Mater. Pavement Des.* 16 (4), 815–835. <https://doi.org/10.1080/14680629.2015.1044558>.
- Pedraza, A., Di Benedetto, H., Sauzéat, C., Pouget, S., 2019. 3D Linear viscoelastic behaviour of bituminous mixtures containing high content of multi-recycled RAP. *Road Mater. Pavement Des.* <https://doi.org/10.1080/14680629.2019.1594054>.
- Pham, N.H., Sauzéat, C., Di Benedetto, H., Gonzalez-Leon, J.A., Barreto, G., Nocolai, A., Jajubowski, M., 2015. RAP and additive influence on 3D linear behaviour of warm bituminous mixtures. *Road Mater. Pavement* 16 (3), 569–591. <https://doi.org/10.1080/14680629.2015.1021108>.
- Phan, C.V., Di Benedetto, H., Sauzéat, C., Lesueur, D., Pouget, S., Olard, F., Dupriet, S., 2017. Complex modulus and fatigue resistance of bituminous mixtures containing hydrated lime. *Construct. Build. Mater.* 139, 24–33. <https://doi.org/10.1016/j.conbuildmat.2017.02.042>.
- Pouget, S., Sauzeat, C., Di Benedetto, H., Olard, F., 2010. From the behavior of constituent materials to the calculation and design of orthotropic bridge structures. *Road Mater. Pavement Design [Special Issue: EATA 2010]* 11, 111–144. <https://doi.org/10.3166/RMPD.11HS>.
- Safavizadeh, S.A., Wargo, A., Guddati, M., Kim, Y.R., 2015. Investigation of reflexive cracking mechanisms in grid-reinforced asphalt specimens using four-point bending notched beam fatigue tests and digital image correlation. *Transport. Res. Rec.* 1998 (2507), 29–38. <https://doi.org/10.3141/2507-04>.
- Saride, S., Kumar, V.V., 2019. Estimation of service life of geosynthetic-reinforced asphalt overlays from beam and large-scale fatigue tests. *J. Test. Eval.* 47 (4), 2693–2716. <https://doi.org/10.1520/JTE20170605>.
- Solatiyan, E., Bueche, N., Carter, A., 2021. Mechanical characterization of grid-reinforced interfaces within rehabilitated bituminous layers. *Construct. Build. Mater.* 288 <https://doi.org/10.1016/j.conbuildmat.2021.122989>, 122989, ISSN 0950-0618.
- Tschegg, E.K., 1986. Test method for the determination of fracture mechanics properties". Patent Specification No. A-233/86 390 328, Austrian Patent Office 1986, Prüfeinrichtung zur Ermittlung von bruchmechanischen Kennwerten sowie hierfür geeignete Prüfkörper, Österreichisches Patent AT- 390328 (In German).
- Tschegg, E.K., Jamek, M., Lugmayr, R., 2012. Crack growth behaviour in geosynthetic asphalt interlayer systems. *Road Mater. Pavement Des.* 13 (1), 156–170. <https://doi.org/10.1080/14680629.2011.644414>.
- Zofka, A., Maliszewski, M., Maliszewska, D., 2016. Glass and carbon geogrid reinforcement of asphalt mixtures. *Road Mater. Pavement Des.* <https://doi.org/10.1080/14680629.2016.1266775>.